

# How Does Flow Rate Affect Drillstring Vibrations? Experimental Investigation

Eshan K. Maitra and Mohammed F. Al Dushaishi, Oklahoma State University

Copyright 2023, AADE

This paper was prepared for presentation at the 2023 AADE National Technical Conference and Exhibition held at the Bush Convention Center, Midland, Texas, April 4-5, 2023. This conference is sponsored by the American Association of Drilling Engineers. The information presented in this paper does not reflect any position, claim or endorsement made or implied by the American Association of Drilling Engineers, their officers or members. Questions concerning the content of this paper should be directed to the individual(s) listed as author(s) of this work.

#### **Abstract**

Drillstring vibration is an unavoidable detrimental dynamic response due to continuous acting external forces and dynamic loading applied during the drilling operation. It constantly works against drilling efficiency and is one of the primary reasons behind downhole equipment malfunctioning, premature fatigue failure, unwanted wellbore enlargement, and deviation from the drilling target. Thus, it is crucial to understand and model the vibration dynamics to develop heuristic vibration mitigation The majority of downscaled experimental investigations provide limited insight into specific vibration mechanisms and cannot address the overall dynamics seen in field conditions. Especially, due to the difficulty of experimental implementation and instrumentation, the integration of circulating fluid has often been ignored; even though, drilling operations are performed under submerged hydrodynamic conditions to maintain wellbore structural stability and mechanical integrity of downhole equipment. The test assembly unveiled in this paper addresses all the above-mentioned issues and encompasses the necessary experimental practices. In this paper, the effect of fluid flow rate on the stability of drillstring vibrations is investigated experimentally using a scaled 20 ft long deviated bottom hole assembly under axial bit interaction using a digitally programmable electromagnetic mechanical shaker. Instead of a general observation of the vibration-damping effect in the presence of circulating fluid, the experiment also presents correlations between vibration characteristics. The novel fully mechanically scaled design allows direct relatability between the experimental responses and real-life field parameters.

#### Introduction

Drillstring (DS) vibration is one of the most detrimental issues for drilling inefficiency. Drilling and exploration for the extraction of energy such as hydrocarbons and geothermal energy is a destructive process of cutting through the earth's subsurface. The physical configuration of the DS also makes it prone to vibrations (Dareing, 1984). DSs consist of a bottom hole assembly (BHA) and a slender section of connected drill pipes that transfer the driving forces from the surface to the drill bit (Figure 1). BHA generally consists of drill collars, heavyweight drill pipes, drill-bit, various mechanical tools, and measurement/logging while drilling (MWD/LWD) tools. The

BHA is the most dynamically active portion of the DS and is constantly subjected to various external forces. It is even emphasized that adjusting the BHA design and operation alone effectively reduces the probability of any severe mechanical vibration occurrences (Dareing, 1984).

The three basic modes of DS vibrations are longitudinal vibration in the axial direction, torsional vibration on the axis of rotation, and bending or transverse vibration in the lateral directions (Figure 2). While DS vibrations can be classified in individual modes, each vibration conjointly contributes to these hindering phenomena. Experimental results have shown that bending and axial vibrations often couple and lead to additional axial shortening of the DS (Yigit and Christoforou, 2000). Drilling vibrations increase the DS to wellbore contact frequency and accelerate DS component wear.

The nature of the vibration ranges from an expected modulation of motion to highly erratic behavior. Vibration can be explained as the instability from its dynamic equilibrium position (Khalil, 2002). Thus, drilling vibrations are often measured in terms of dynamic displacement over time, or as unintentional erratic acceleration. Such occurrence of dynamic disposition can be characterized through flexural studies and spectral analysis, which are used to identify critical operating frequencies (Dong and Chen 2016). Avoidance of these operational critical frequencies or system eigenvalues of a DS assembly reduces the probability of premature catastrophic failure of the downhole components and enhances the overall drilling performance (Bailey et al., 2016).

Several practical heuristic DS vibration mitigation strategies have been proposed over decades (Ghasemloonia et al., 2015). But there have not been enough investigations on the effects of fluid presence during the drilling operation. Theoretically, fluid-induced vibrations of DS have been addressed in multiple forms (Paidoussis et al., 2008). But very few address its application for drilling vibration (Al Dushaishi et al., 2016). Due to the difficulty of experimental implementation, and instrumentation, the presence of fluid is often ignored in the experimental investigations of drilling vibrations.

Most of the past experimental investigations that are relatable to DS vibration conducted flexural analysis for confined rotor dynamics under partially or fully fluid submersion; following the theory of hydrodynamic mass effects on dynamic bodies originally proposed by Stokes (1843). Fritz (1970) formulated an

experimental vibration study of a flexible supported rotor with a small degree of unbalance, surrounded by a thin layer of fluid. The experiment included a 1.125 in diameter and 6 in long vertical aluminum rotor representing the DS within a larger steel container acting as the wellbore, with a radial clearance of about 0.2 in. A 1-HP DC motor was used as the top-drive, and a wooden mallet was used to create sharp impulse shocks to the rotor. Fluid damping effects for air, water, oil, and water-glycerol mixture were investigated. The radial deflection, rotational vibration amplitude, and natural frequencies of the system were measured and compared, with and without rotation.

Similarly, in 1992, Antunes et al. used a large experimental setup of a rotor to investigate the lateral vibration dynamics including different whirling, under submerged conditions. A vertical rotor shaft of 3 ft could be partially or fully submerged in fluids within clear cylindrical confinement. Struts were used for rotor stabilization, and a shaker was used to apply lateral excitation from the top. They investigated the damped vibration response due to added mass of the fluid, fluid viscosity, and fluid friction, for different submersion levels of fluid. The result showed a parabolic relation between the critical velocity and the fluid level.

One of the first laboratory scaled experiments of DS vibrations under submerged conditions was conducted by Berlioz et al., (1996). They experimented with two different DS assemblies, one fully vertical and one deviated. A slender 0.12 in diameter steel rod, with 58.46 in straight length and 74 in curved section with stabilizers, represented the experimental DS. Water-tight removable plexiglass pipes of different diameters were installed around the DS to mimic the wellbore with different annulus clearances. The rig was remodeled from a small vertical drill machine that operated at a maximum of 150 RPM. A shaker was used to simulate the bit rock interaction from the bottom end to induce lateral instability. The results showed that increasing fluid density and viscosity decrease the lateral frequency and reduce the vibration levels through dissipation. This experimental investigation validated several other previous assumptions.

Khulief and Sulaiman (2009) verified their fluid elastodynamic model with another experiment and spectral analysis. The experiment consisted of a uniform steel rod of 0.24 in diameter with an effective length of 56.7 in resembling a vertical BHA. A magnetic tension brake and electromagnetic shakers were used to simulate the bit rock interaction in the torsional and axial directions. The DS rod ran through a plexiglass tube resembling a wellbore filled with air, turpentine oil, or water. Water-tight eddy current proximity probe stations were placed at equal distances onto the plexiglass to measure the vibratory deflection. They recognized that the fluid friction depends on the oscillation frequency of the vibrating elastic structure and decreases with the frequency of the axial load throughout the DS.

Although all these investigations provided more practical insight into the effects of different fluids on DS vibrations and how the presence of fluid affects some operational conditions, they neglected the effect of fluid circulation and hydrodynamic pressure variance in the annulus section.

## Methodology

Most laboratory scaled experimental studies only aim to establish the mathematical relation for the research-specific assembly based on the recreation efficiency of the vibration phenomena under study. However, only geometric, or arbitrary dynamic scaling isolates the study to replicate vibration mechanisms that would occur under specific conditions and therefore limits direct correlations with field-size operations. Hence, recreating the vibration phenomenon on a mechanically scaled experiment with the operational parameters scaled from the field-size operations would result in the observation and measurement of more accurate dynamic responses.

Shyu (1989) presented the first comprehensive dimensional analysis for an experimental setup of DS lateral vibration in the light of mechanical scaling that incorporated relations between the scaling of geometry, material properties, and internal and external forces. Shyu's (1989) scaling approach represented the BHA by simplified drill collars, where the Buckingham Pi Theorem was constructed for the drill collars using ten parameters affecting the DS lateral vibration (Eq. 1).

$$s = f(l, d, D, E, \rho, \rho_m, T, g, \phi, \Omega)$$
 (Eq. 1)

Here, s denotes the lateral displacement of the drill collar, l is the characteristics length of the drill collar, d is the drill collar outside diameter, D is the diameter of the borehole, E is the drill collar's Young's modulus, T is the weight on bit, g is the acceleration due to gravity,  $\phi$  is the borehole slant angle,  $\Omega$  is the collar's rotational speed,  $\rho$  and  $\rho_m$  are the drill collar and mud density respectively.

Using three independent parameters namely, l with a dimension of L length,  $\rho$  with dimensions of  $M.L^{-3}$ , and E with dimensions of  $M.S^{-2}.L^{-1}$  where S denotes time, the Buckingham $\pi$  was used to establish non-dimensional relationships as seen in Eq. 2.

$$\frac{s}{l} = f^*(\theta_1, \theta_2, \theta_3, \theta_4, \theta_5, \theta_6)$$
 (Eq. 2)

Here,  $\theta_1$ =d.l<sup>-1</sup>,  $\theta_2$ =D.l<sup>-1</sup>,  $\theta_3$ =T.l<sup>-2</sup>.E,  $\theta_4$ =E.g<sup>-1</sup>.l<sup>-1</sup>.( $\rho$ - $\rho_m$ ),  $\theta_5$ =l. $\Omega$ .(( $\rho$ - $\rho_m$ ).E<sup>-1</sup>)<sup>1/2</sup>, and  $\theta_6$ = $\phi$ .

In terms of the independent variables, scaling ratios and operational parameters similarity relating the laboratory prototype to the real model are derived and summarized in Eq. 3, where "P" and "M" subscripts denote the prototype and model respectively.

$$\frac{d_M}{d_P} = \lambda_1 \qquad \frac{D_M}{D_P} = \lambda_1 \qquad (Eq. 3)$$

$$\frac{T_M}{T_P} = \frac{(l^2 E)_M}{(l^2 E)_P} = \lambda_1^2 \lambda_3 \qquad \frac{(\rho - \rho_m)_M}{(\rho - \rho_m)_P} = \frac{E_M l_P}{E_P l_M} = \frac{\lambda_3}{\lambda_1}$$

$$\frac{\phi_M}{\phi_P} = 1 \qquad \frac{\Omega_M}{\Omega_P} = \frac{\left[l(\frac{\rho - \rho_m}{E})^{\frac{1}{2}}\right]_P}{\left[l(\frac{\rho - \rho_m}{E})^{\frac{1}{2}}\right]_M} = \frac{\left(\frac{\lambda_3}{\lambda_1 \lambda^2}\right)^{\frac{1}{2}}}{1}$$

Where the notation ratios are defined as  $\lambda_1 = \frac{l_M}{l_P}$ ,  $\lambda_2 = \frac{(\rho - \rho_m)_M}{(\rho - \rho_m)_P}$ , and  $\lambda_3 = \frac{E_M}{E_P}$ . Several researchers presented methods of mechanical and dynamic scaling of unbalanced rotor bodies, however, very few bridged the relation for DS operations.

# **Experimental Setup**

A novel mechanically downscaled test assembly adhering to the geometric and material property relations of a horizontal BHA section was designed and manufactured to recreate and investigate the nature of lateral vibration phenomena under drilling action, i.e., induced axial-rotational excitation, using an electromagnetic shaker and an electrical motor (Figure 3 and Figure 4). Table 1 shows the scaling relations between the experiment and the field scale.

**Table 1: Mechanical Scaling Information** 

BHA Scaling Factors		$\lambda_1$	$\lambda_2$	$\lambda_3$	
		0.061	0.119	0.002	
		Unit	Field Equivalent	Experiment	
Geometric	Outside Diameter	in	6.75	0.625	
	Inside Diameter	in	4	0.5	
	Length	ft	328.1	20	
Material	Density	lb.ft <sup>-3</sup>	490	58.7	
	Elasticity	psi	3.00E+07	6.70E+04	
Dynamic	Rotation	RPM	157	350	
		RPM	314	700	

A single-axis high-frequency accelerometer was fitted to the electromagnetic shaker to create a feedback loop to ensure desired induced axial force was applied. A high-frequency triaxial accelerometer was placed at the bit section for real-time observation and recording of the drilling dynamics data.

#### Test Matrix

Sine-sweeps were conducted using the electromagnetic shaker with a maximum force of 18 g. Peak-to-peak displacement or axial motion was fixed at rotational speeds of 0, 350, and 700 rotation per minute (RPM) runs. Thus, the applied force varied during the full sweep – reaching maximum motion at the highest frequency and gradually decreasing over time as frequency reduced. The sweep rate was 12 Hz per minute. Each case was run without flow at 0 gallons per minute (GPM), 0.75 GPM, and 1.15 GPM. The average wellbore pressures were 13 psi and 15 psi respectively for 0.75 GPM and 1.15 GPM. Only water was used for this experiment. Table 2 summarizes the testing matrix for the different rotational speeds and applied displacement and excitation frequencies.

**Table 2: Test Matrix** 

Flow Rate [GPM]	0	0.75	1.15
	Displacement [in]	Rotation [RPM]	Max Sweep Frequency [Hz]
Case# 1		0	
Case# 2	0.2	350	30
Case# 3		700	
Case# 4		0	
Case# 5	0.075	350	
Case# 6		700	60
Case# 7		0	00
Case# 8	0.05	350	
Case# 9		700	
Case# 10		0	
Case# 11	0.025	350	120
Case# 12		700	

#### **Results and Discussion**

The experimental data consists of the drillstring acceleration response magnitudes in the three-coordinate system measured at 100kHz. Figures 5 and 6 show the applied acceleration and the BHA acceleration responses in the x, y, and z directions of Case 5 and Case 8, respectively, for the different flow rates at 350 RPM, over a full sine-sweep. Both Figure 5 and Figure 6 represent a sine-sweep that achieves a maximum sweep frequency of 60 Hz around 10 seconds mark and gradually decreases the frequency of the axial excitation until reaching near 0 Hz at a 12 Hz per minute sweep rate. The axial excitations displacements were 0.075 in and 0.05 in respectively for Case 5 and Case 8. For both cases, the BHA response in the x-direction is similar to the induced axial vibration, besides a few random noises and possible high-frequency coupled vibration responses. This is mainly due to the BHA response in the x-direction being measured close to the applied excitation as shown in the experimental setup in Figure 3. From the flow rate effect point of view, it can be seen that the acceleration amplitude for 0 GPM is higher than 0.75 and 1.15 GPM for both cases. For the BHA response in the y-direction, Case 5 (Figure 5) shows lower vibration amplitude compared to the x-direction, while the flow rate effect shows different behavior for the high and lowfrequency excitations. For instance, at high excitation frequency, the vibration amplitude of the 0.75 GPM is higher than the other cases, while at low vibration amplitude, the 0 GPM test shows the highest vibration amplitude. A similar trend can be seen for Case 8 (Figure 6), however, the vibration amplitude for the 1.75 GPM was the highest in the high excitation frequency range. The BHA response in the z-direction for Case 5 (Figure 5) shows the same behavior seen in the y-direction vibration amplitude. However, Case 8 (Figure 6) shows the vibration amplitude in the y-direction for the 0 GPM test being the highest across the excitation frequency spectrum.

It is to be noted that, due to the general design of the horizontal wellbore, the experimental BHA mostly lays on the wellbore low side and comes in contact with the wellbore more often in the z-direction, which matches filed case observations.

Therefore, compared to the *x* or *y*-direction responses, the *z*-direction acceleration responses are not fully symmetric for both Case 5 (Figure 5) and Case 8 (Figure 6).

For more insights into the BHA dynamics, the tri-axial vibration response data was processed using the Power Spectral Density (PSD) to investigate the effect of flow rate on the frequency response spectrums. Figure 7 shows the PSD spectrum of Case 5 in the x, y, and z directions for the different flow rates. In the axial direction, Figure 7-a1-a3, the flow rate shows a minimum effect, i.e. no change in dominant frequency, on the PSD spectrum at the low and high-frequency range. At the low range, Figure 7-a2, a damping effect due to fluid flow can be seen at approximately 12 Hz. In the high-frequency range, increasing the flow rate causes an increase in the spectral energy at approximately 50 Hz (Figure 7-a3). In the lateral directions, i.e., the y and z, due to symmetry, the PSD spectrums of both directions are similar (Figure 7-b-c). The fluid flow shows an increase in the spectral energy in the low range of frequency below 15 Hz as seen in Figure 7-b2&c2. At the higher frequency range, the fluid flow shows a damping effect (Figure 7-b3&c3).

The PSD response of the BHA for Case 8 is shown in Figure 8 for the different flow rates. In the *x*-direction, similar behavior to case 5 (Figure 7) can be seen at the lower frequency range with an increase in the spectral energy below 15 Hz (Figure 8a-2). At the high frequency range the fluid flow shows a damping effect with lower PSD response, however, the change in flow rate from 0.75 to 1.15 GPM shows a minimal change in damping ratio (Figure 8-a3). In the lateral directions, i.e., *x* and *y* response, the PSD spectrum shows similar behavior seen in Case 5, where the flow rate caused an increase in the energy spectrum at the low frequency range (Figure 8-b2&c2) and a damping effect with a small shift in dominate frequency at the high frequency range (Figure 8-b3&c3).

The axial excitations displacements of Case 5 and Case 8 were 0.075 in and 0.05 in, respectively. Comparing the *y*-direction responses of Case 5 (Figure 7-b3) and Case 8 (Figure 8-b3), it can be seen that both flow conditions were more effective in damping the vibration for Case 8 with lower axial excitation levels. This is more evident while comparing the *z*-direction responses of Case 5 (Figure 7-c3) and Case 8 (Figure 8-c3).

### Flow Rate Effect on Vibration Response

The effect of flow rate was investigated at different excitation levels and rotational speeds as presented in Table 2. Figure 9 through Figure 20 shows the PSD response of the lateral acceleration in the *y* and *z* directions for Case 1 through Case 12, respectively. A summary of the vibration response observations seen for each case is presented in Table 3.

The first cases from Case 1-3 (Figure 9-11) represent cases with the highest axial peak-to-peak excitation. It has been mentioned that the maximum allowable axial excitation was provided up to the limitation of the electromagnetic shaker. As the applied excitation frequency increases more axial force is required for a fixed axial peak-to-peak excitation. Thus, the maximum applied axial excitation frequency for Cases 1-3 was 30 Hz (Figures 9-11).

Cases 1-3 (Figure 9-11) show that flow rate amplifies vibration amplitude at low frequency and flow dampens vibration in the high frequency range, with low flow rate being more effective in vibration damping (Figure 9-a3&b3). The vibration response peaks are larger at the higher RPM range in Case 3 (Figure 11-a2&b2), and similarly, fluid flow exhibits higher vibration-damping effectiveness (Figure 11-a3&b3). It can also be observed that a higher flow rate shifts the frequency of peak responses further to the lower range (Figure 9-a1,a3,b1&b3).

It can be said that the circulating fluid does not just dampen the vibratory responses. Fluid presence shifts the harmonic frequency of the system to a lower frequency. It is to be emphasized that a lower value of frequency does indicate a lower level or rank of critical condition. The occurrence only takes place at a different frequency. The critical vibratory response with high magnitude can still be observed, which can be just as detrimental or catastrophic if not avoided.

The effect of a higher flow rate in vibration damping becomes clearer when observed within a broader frequency window of vibration responses, as in Case 4-9 (Figure 12-17). It can be seen that, higher flow rate aid in damping vibration amplitudes in the higher frequency range, especially in the *y*-direction (Figure 12-17-a3). Flow seems to have less effect in the *z*-direction while viewing in the narrow windows of Figure 12-17-b3. But a higher flow rate shows an overall less vibration response while viewing the entire response spectrum in Figure 12-17-a1&b1.

Comparing Case 7 (Figure 15-a3&b3) and Case 4 (Figure 12-a3&b3) it is observed that flow is more effective in reducing overall erratic vibration in the lower axial excitation cases. Especially, Case 7 (Figure 15-a1&b1) exhibits no large acceleration peaks due to flow at a low frequency range. In Case 4-9 (Figure 12-17-a1&b1) the high vibration response between 55-60 Hz due to flow is expected to be observed due to a shift in the frequency of peak responses or harmonics of the system. Since a high flow rate effectively reduces the value of the first harmonic frequency to a lower frequency, the harmonics become more frequent within a set window of observed frequencies. This also results in the observation of higher vibration peaks for high flow rate conditions at a lower frequency range.

The consistent damping efficiency and the nature of shifting frequencies of peak vibration responses or harmonic is most evident in Case 10-12 (Figure 18-20). The 0.75 GPM flow rate is more effective in damping vibration in the lower frequency range (Figure 18-20-a3). The 1.15 GPM is more effective in the higher frequency range (Figure 18-20-b3) except for one irregular vibration response observed between 75-85 Hz in the z-direction of Case 10 (Figure 18-b3). Comparing the 0 GPM flow condition to the 1.15 GPM case at high frequency window of 90-100 Hz (Figure 11-a3&b3), shifts and damped vibration peaks plateau over a range of frequencies instead of exhibiting large-concentrated peaks at specific frequencies.

A higher flow rate is more consistent in damping vibration, especially for high-frequency vibratory responses. As a result, sudden high vibration peaks are rare in the high frequency range for higher flow rate conditions.

Table 3: Observation Summary Lateral Accelerations PSD Responses in the y And z Directions of all Cases

Case	Excitation (in)	RPM	Vibration Response Observations
Case 1 Figure 9		0	Flow rate increases vibration amplitude at low frequency (Figure 9-a2&b2) and flow dampens vibration in high frequency zones, with low flow rate being more effective (Figure 9-a3&b3). Higher flow rate shift frequency of peak responses further to the lower range (Figure 9-a1,a3,b1&b3).
Case 2 Figure 10	0.2	350	Excitation amplification at low frequency at 12-13 Hz (Figure 10-a2&b2). Vibration dampening and frequency shift due to flow is observed for peak responses at higher frequency zone (Figure 10-a1,a3,b1&b3).
Case 3 Figure11		700	Similar to Case 1 and Case 2. But peak vibration amplitudes are larger everywhere at higher RPM. Similarly, fluid flow exhibits higher vibration damping effectiveness.
Case 4 Figure 12		0	Frequency shift can be observed (Figure 12-a2&b2). Overall, higher flow rate is more effective in vibration damping in high frequency range but, high vibration amplitudes are observed between 55-60 Hz (Figure 12-a1&b1).
Case 5 Figure 13	0.075	350	Similar to Case 4. Flow is more consistent in damping overall vibration except between 55-60 Hz (Figure 13-a1&b1). Vibration amplitudes peak for rotation around 12 & 17 Hz (Figure 13-a2&b2).
Case 6 Figure 14		700	Similar acceleration peak response as Case 5, along with additional erratic peaks (Figure 14-a2&b2). More effective damping was observed in the <i>y</i> -direction.
Case 7 Figure 15		0	Similar frequency observation window as Case 4 (Figure 12) and shows similar nature in low frequency zone (Figure 15-a2&b2). But exhibits no large acceleration peaks due to flow (Figure 15-a1&b1). Flow is more effective in reducing overall vibration in this low axial excitation case (Figure 15-a3&b3). Except for one irregular jump for 0.75 GPM in the z-direction (Figure 15-b1).
Case 8 Figure 16	0.05	350	Similar vibration responses as Case 5 (Figure 13) but, flow exhibits comparatively more effectiveness in overall damping in this case of lower axial excitation (Figure 16).
Case 9 Figure 17		700	Similar comparison can be stated between Case 6 (Figure 14) and Case 9 (Figure 17), as seen between Case 5 (Figure 13) and Case 8 (Figure 16). But the irregular z-direction vibration amplification is absent in Case 9 (Figure 17-b3) compared to Case 6 (Figure 14-b3).
Case 10 Figure 18		0	Vibration dampening and frequency shift due to flow are more evident. 0.75 GPM is more effective in damping vibration in the lower frequency range and 1.15 GPM is more effective in the higher frequency range. Except for one irregular vibration response observed between 75-85 Hz in the z-direction (Fig.18-b3).
Case 11 Figure 19	0.025	350	Erratic vibration responses are prominent in this higher RPM case (Figure 19) than the previous case (Figure 18). Shifted and damped vibration peaks plateau at a higher frequency due to flow over a range of frequencies, as seen between 90-100 Hz for 1.15  GPM flow (Figure 11-a3&b3)
Case 12 Figure 20		700	Erratic behavior further increases due to higher RPM but, similar characteristics are more prominent, compared to Case 10 and Case 11.

#### **Conclusions**

A mechanically scaled experimental investigation was presented to study the effect of flow rate under axial vibration and rotation on drillstring lateral vibrations. The experimental observation showed –

- 1. Higher flow rates are more consistent in smoothing overall erratic vibration chatter and more effective in damping vibration at a higher frequency.
- 2. As the flow rate increases, a shift in peak frequencies of vibration responses to the lower frequency range is observed. As a result, a higher flow rate increases peak vibration responses in the lower frequency zones.
- 3. Higher flow rate restricts amplitudes of peak vibration responses and plateaus high magnitude responses over a range of frequencies.

Due to experimental limitations, the axial force could not be applied and observed at high frequencies for all the cases and the experiments were conducted only for low flow rates. Yet, the robust experimental system established a practical and precise understanding of the effect of fluid flow on the drilling vibrations.

#### References

- Al Dushaishi, M. F., Nygaard, R., and Stutts, D. S. 2016. "Effect of drilling fluid hydraulics on drill stem vibrations." Journal of Natural Gas Science and Engineering, 35, p. 1059-1069. <a href="https://doi.org/10.1016/j.jngse.2016.09.041">https://doi.org/10.1016/j.jngse.2016.09.041</a>
- Antunes, J., Axisa, F., and Hareux, F. 1992. "Flexural vibrations of rotors immersed in dense fluids Part II: Experiments." Journal of Fluids and Structures, 6(1), p. 23-38. https://doi.org/10.1016/0889-9746(92)90053-6
- 3. Bailey, J. R., Pastusek, P. E., Junaibi, H. A., Awadhi, M. A., Katheeri, Y. A., Niznik, M. R., ... and Page, C. G. 2016. "An integrated workflow to mitigate drilling vibrations and increase daily footage." In Abu Dhabi International Petroleum Exhibition & Conference. OnePetro. https://doi.org/10.2118/183550-MS
- Berlioz, A., Der Hagopian, J. and Dufour, R. 1996. "Dynamic Behavior of a Drill-String: Experimental Investigation of Lateral Instabilities." J. Vibration & Acoustics, 118(3), p. 292–298. http://dx.doi.org/10.1115/1.2888180
- Dareing, D. W. 1984. "Drill collar length is a major factor in vibration control." Journal of petroleum technology, 36(04), 637-644. https://doi.org/10.2118/11228-pa
- Dong, G., and Chen, P. 2016. "A review of the evaluation, control, and application technologies for drill string vibrations and shocks in oil and gas well." Shock and Vibration, 2016. <a href="https://doi.org/10.1155/2016/7418635">https://doi.org/10.1155/2016/7418635</a>
- Fritz, R. J. 1970. "The Effects of an Annular Fluid on the Vibrations of a Long Rotor, Part 2—Test." ASME. J. Basic Eng. December, 92(4), p. 930–937. https://doi.org/10.1115/1.3425166
- 8. Ghasemloonia, A., Rideout, D. G., and Butt, S. D. 2015. "A review of drillstring vibration modeling and suppression methods." Journal of Petroleum Science and Engineering, 131, p. 150-164. https://doi.org/10.1016/j.petrol.2015.04.030
- Khalil, H. K. 2002. "Nonlinear systems (3rd ed.)." Prentice hall Upper Saddle River.
- Khulief, Y. A., and Al-Sulaiman, F. A. 2009. "Laboratory investigation of drillstring vibrations." Proceedings of the Institution of Mechanical Engineers, Part C: Journal of

- Mechanical Engineering Science, 223(10), p. 2249-2262. https://doi.org/10.1243/09544062JMES15
- Paidoussis, M., Luu, T., Prabhakar, S., 2008. "Dynamics of a long tubular cantilever conveying fluid downwards, which then flows upwards around the cantilever as a confined annular flow." J. Fluids Struct., 24 (1), p. 111-128. http://dx.doi.org/10.1016/j.jfluidstructs.2007.07.004
- Shyu, R. J. 1989. "Bending Vibration of Rotating Drill Strings." PhD dissertation, MIT, Cambridge, Massachusetts.
- Stokes, G. G. 1843. "On Some Cases of Fluid Motion." Proceedings of the Cambridge Philosophical Society, 8, May, p. 105-137.
- 14. Yigit, A. S., and Christoforou, A. P. 2000. "Coupled torsional and bending vibrations of actively controlled drillstrings." Journal of sound and vibration, 234(1), p. 67-83. https://doi.org/10.1006/jsvi.1999.2854

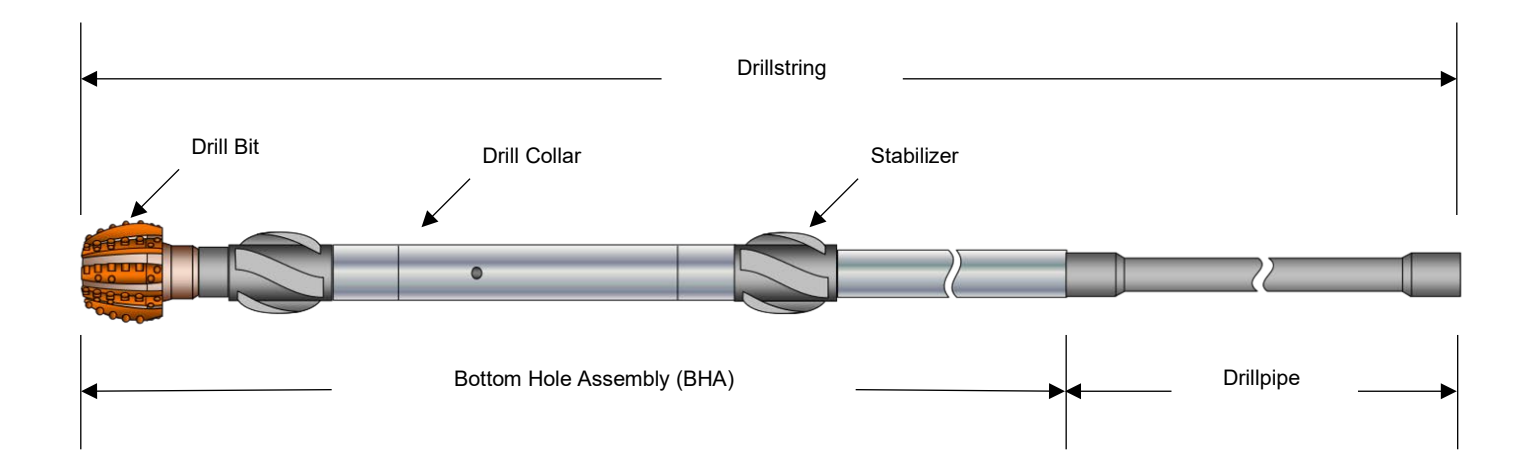


Figure 1 - Drillstring general components

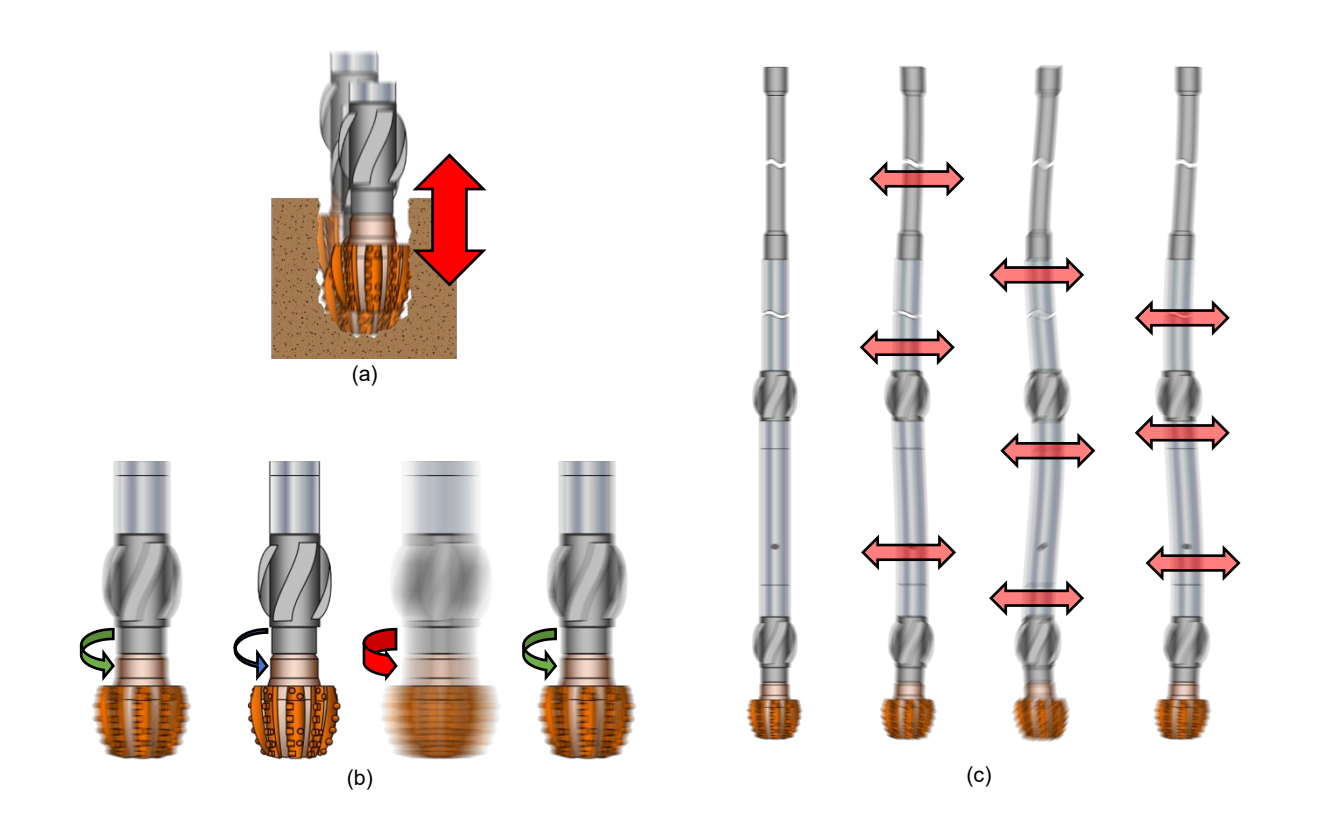


Figure 2 – Drillstring vibration modes: (a) Axial/Bit-Bounce, (b) Torsional/Stick-Slip, and (c) Bending/Whirl

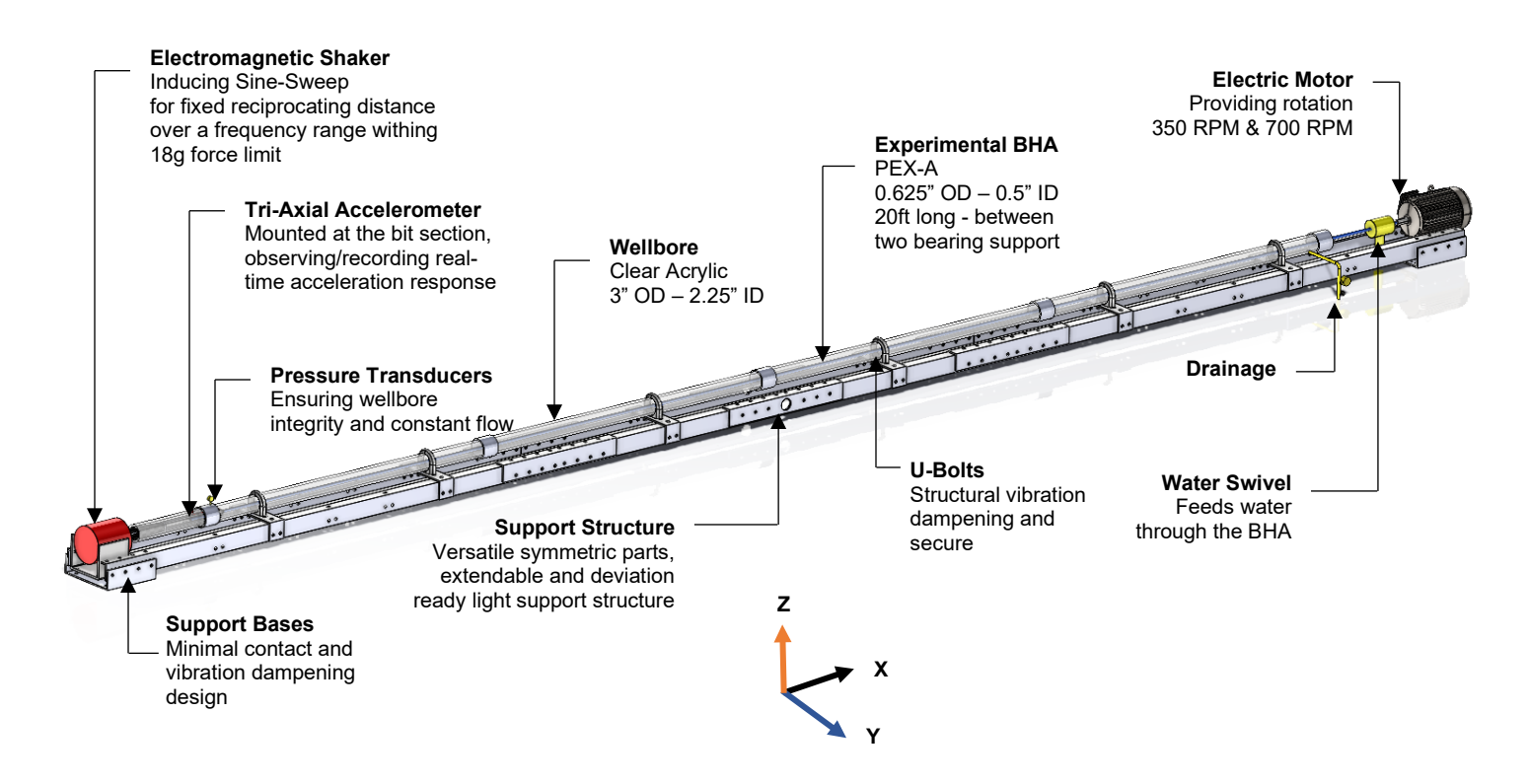


Figure 3 - Design schematic of the experimental setup

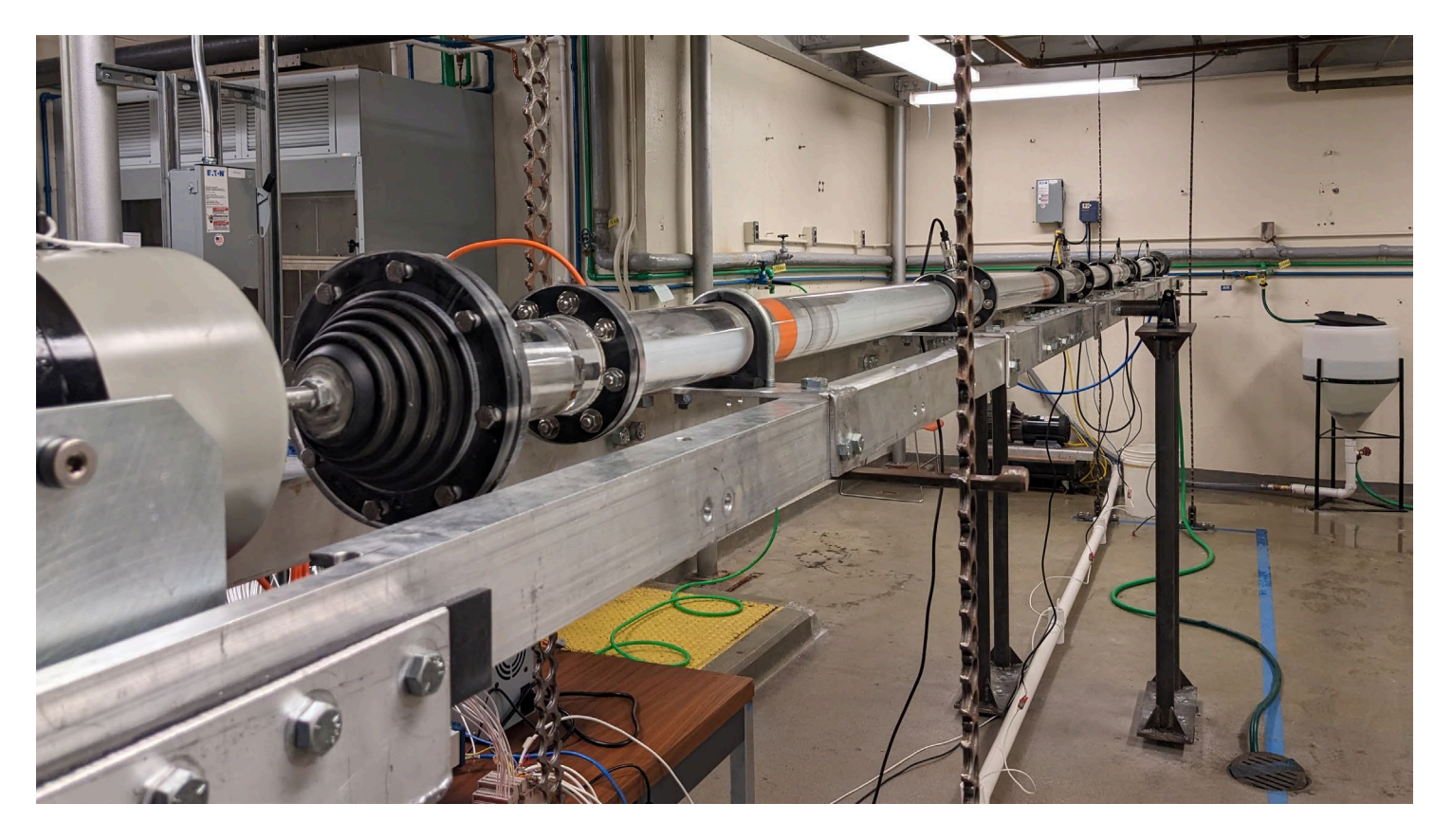


Figure 4 - A photo of the experimental setup

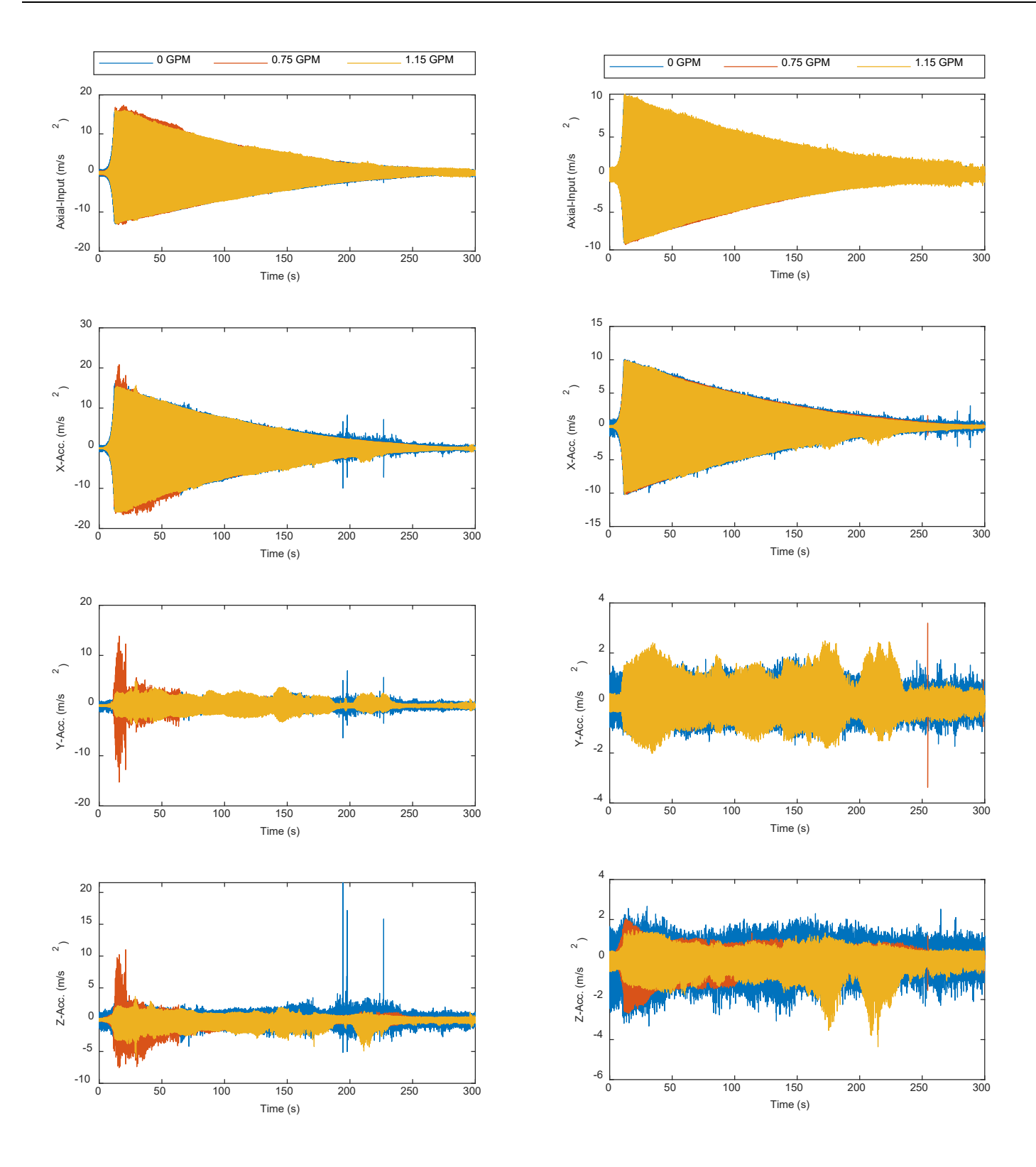


Figure 5 – Case 5 – Acceleration magnitude of induced axial input motion and recorded acceleration response at the bit section for all the coordinates, respectively from top to bottom.

Figure 6 – Case 8 – Acceleration magnitude of induced axial input motion and recorded acceleration response at the bit section for all the coordinates, respectively from top to bottom.

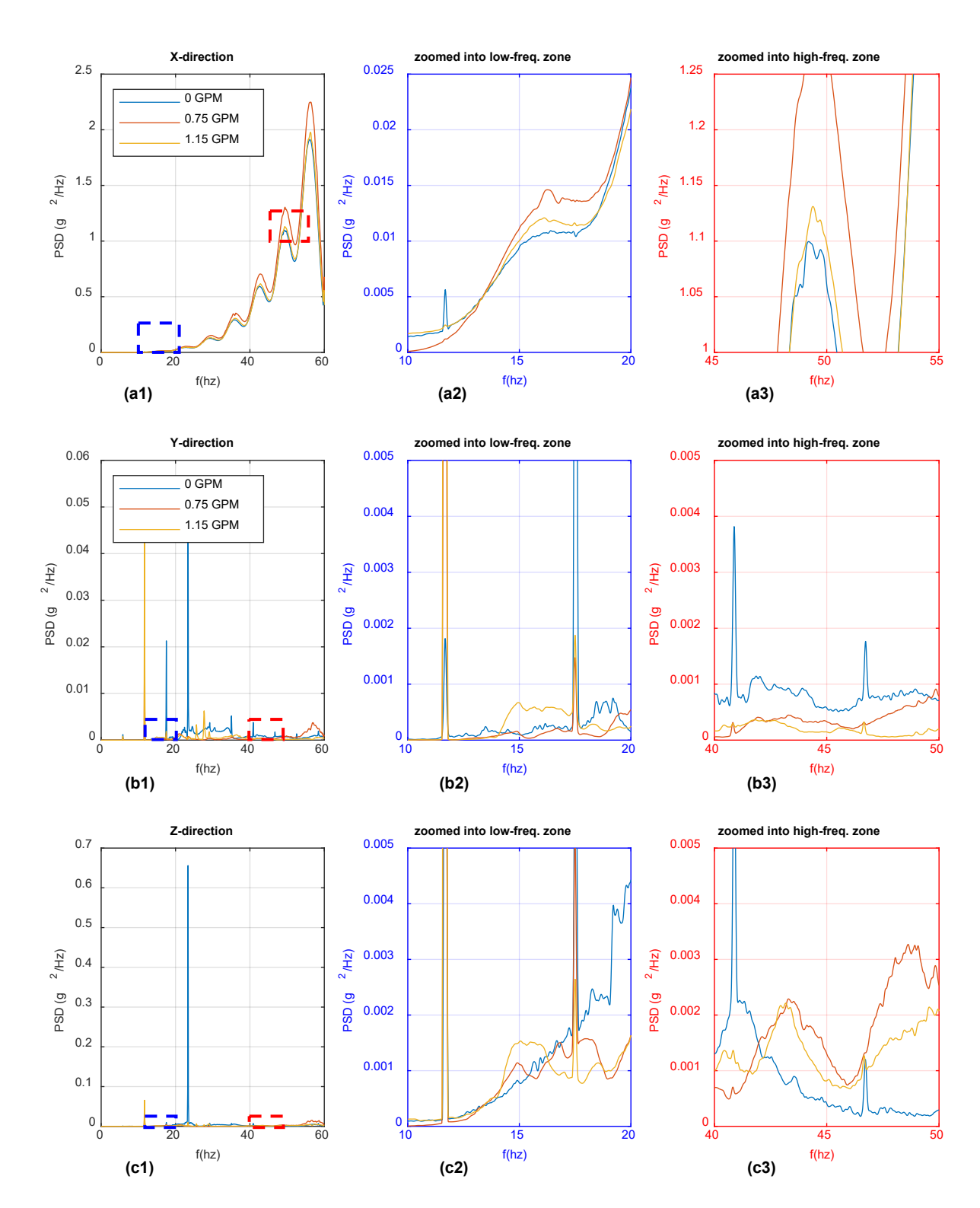


Figure 7 – Case 5 – Power Spectral Density (PSD) of the axial excitation, x, y, and z responses at the bit-section

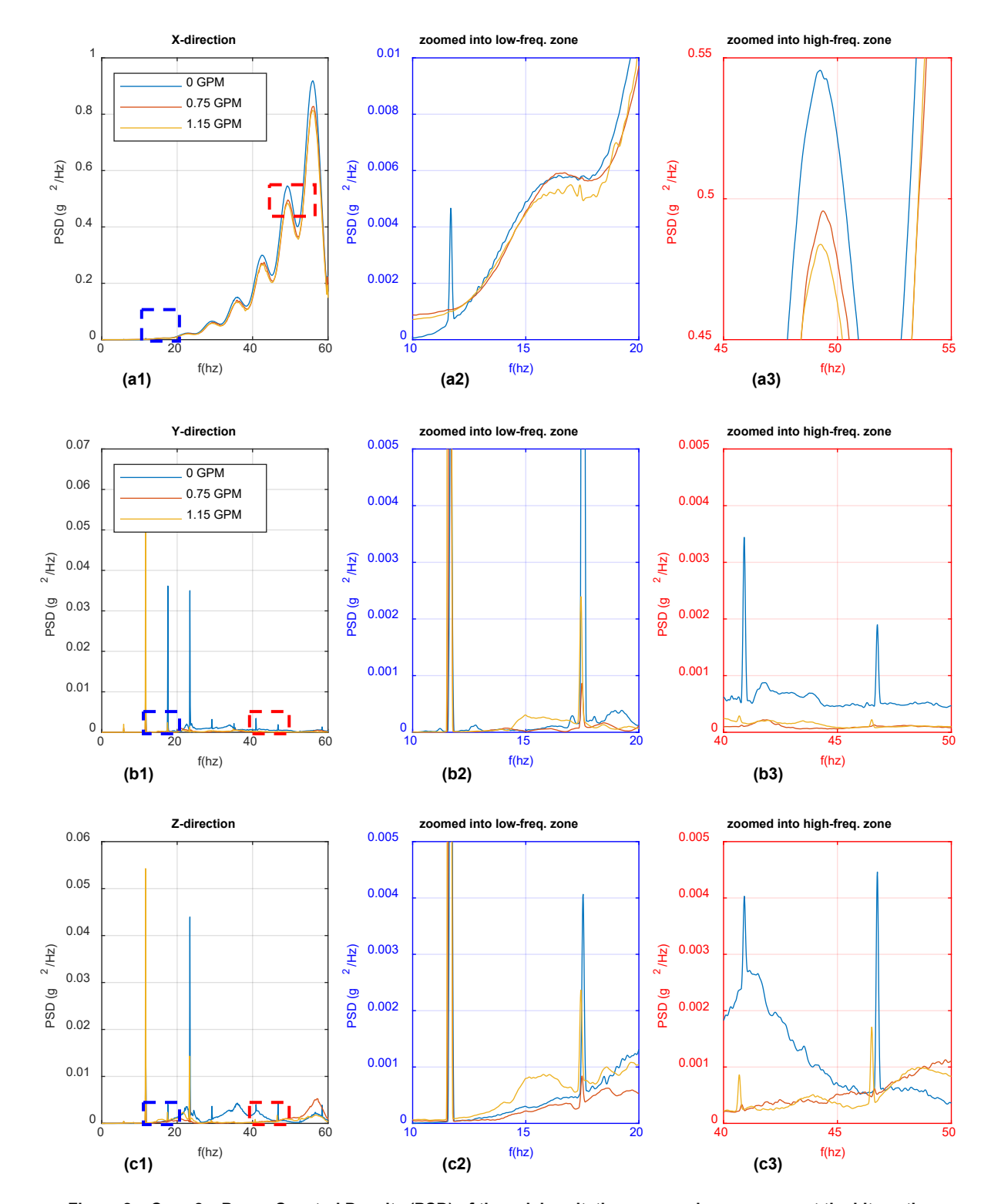


Figure 8 – Case 8 – Power Spectral Density (PSD) of the axial excitation, x, y, and z responses at the bit-section

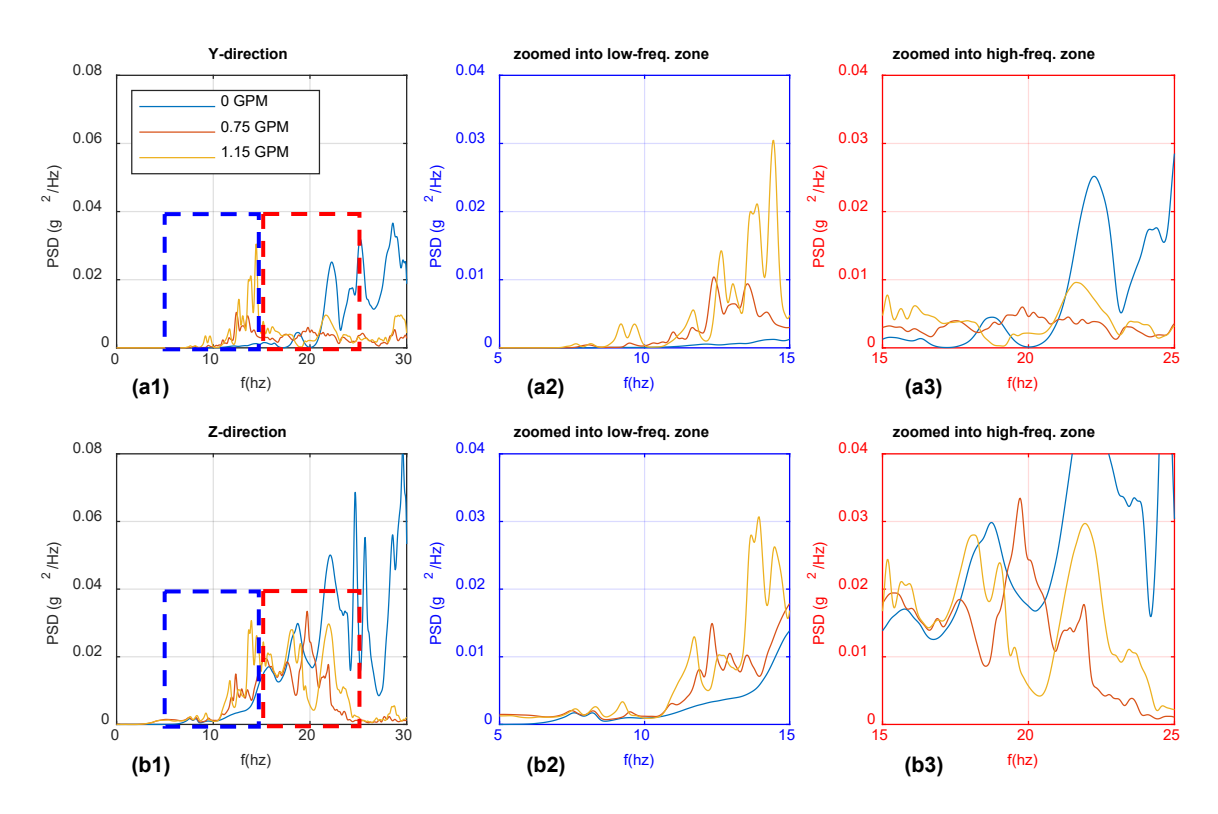


Figure 9 - Case 1 - Lateral acceleration Power Spectral Density (PSD) response for different flow rates in the y & z direction

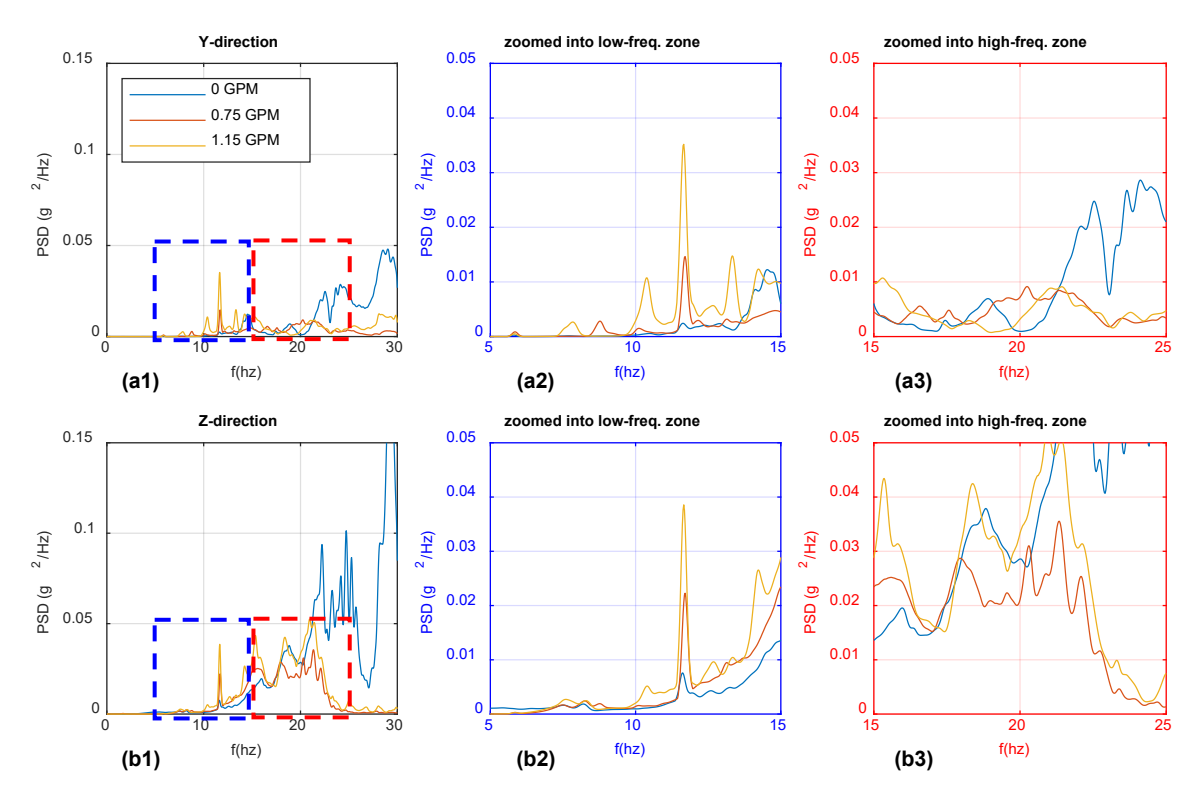


Figure 10 - Case 2 - Lateral acceleration Power Spectral Density (PSD) response for different flow rates in the y & z direction

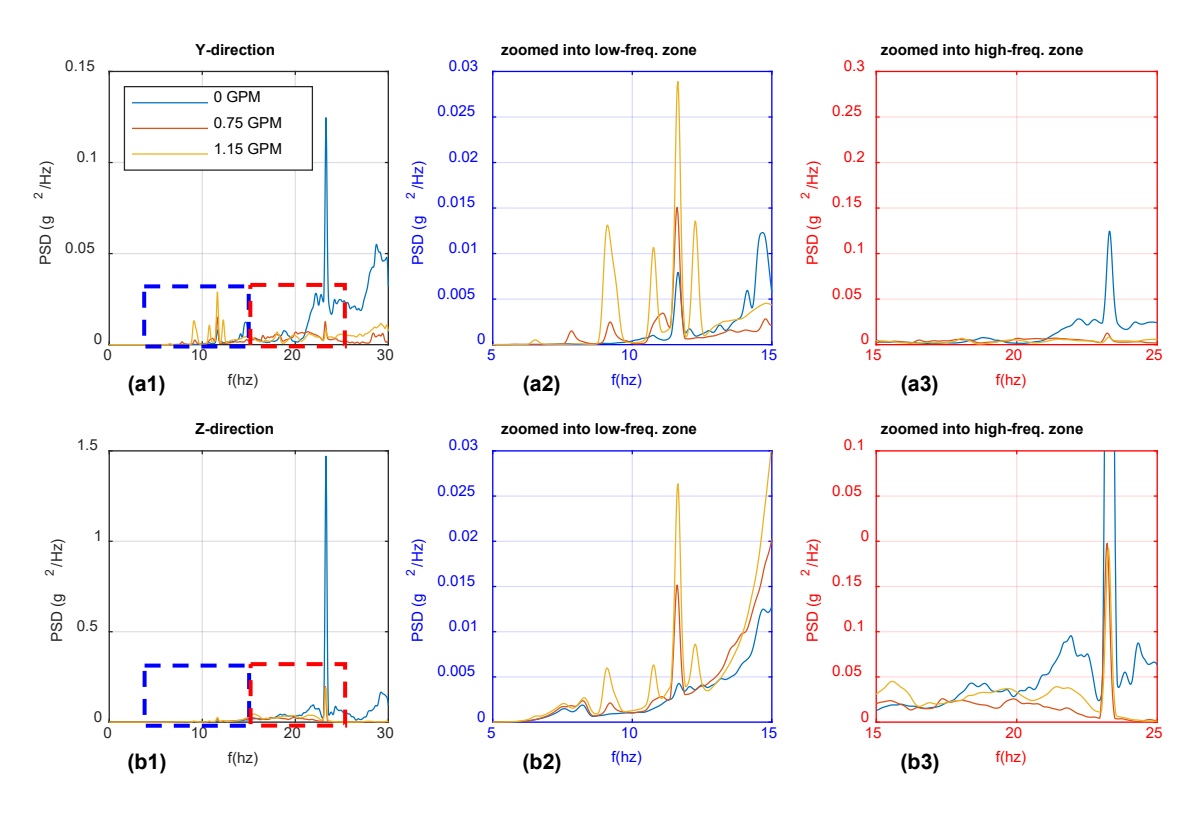


Figure 11 - Case 3 - Lateral acceleration Power Spectral Density (PSD) response for different flow rates in the y & z direction

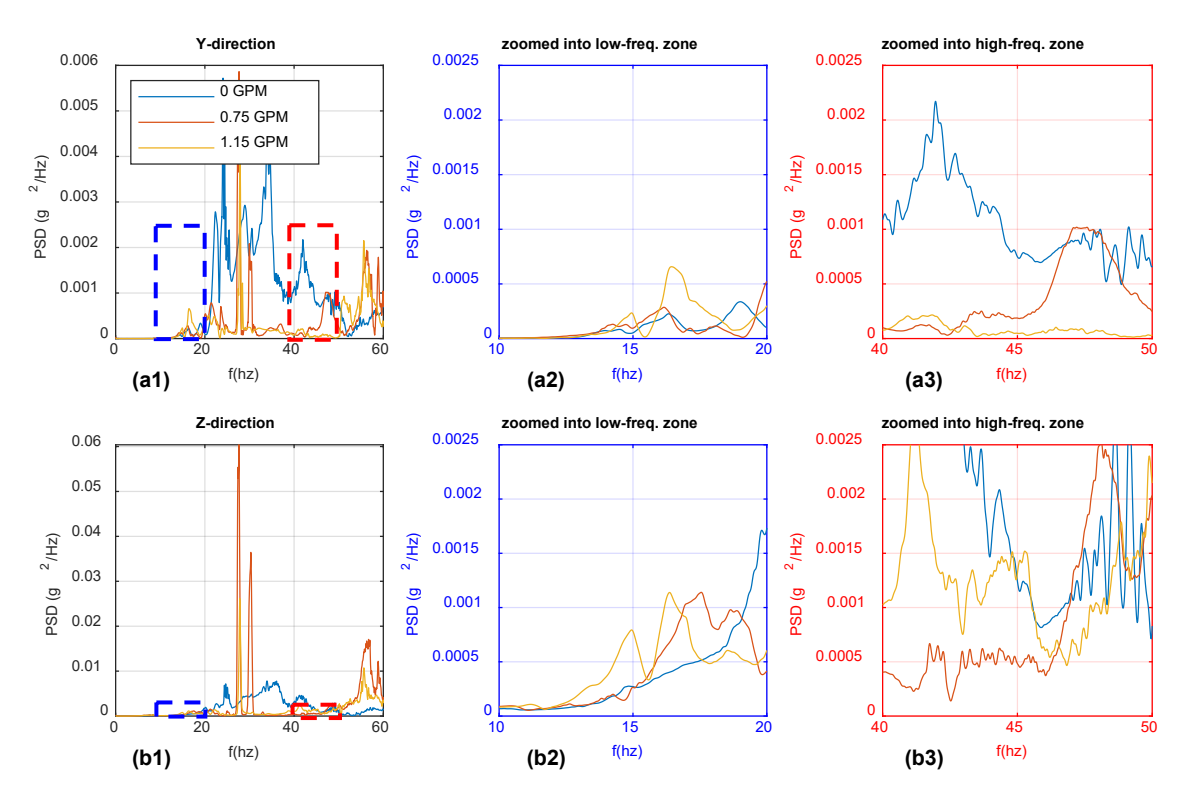


Figure 12 – Case 4 – Lateral acceleration Power Spectral Density (PSD) response for different flow rates in the y & z direction

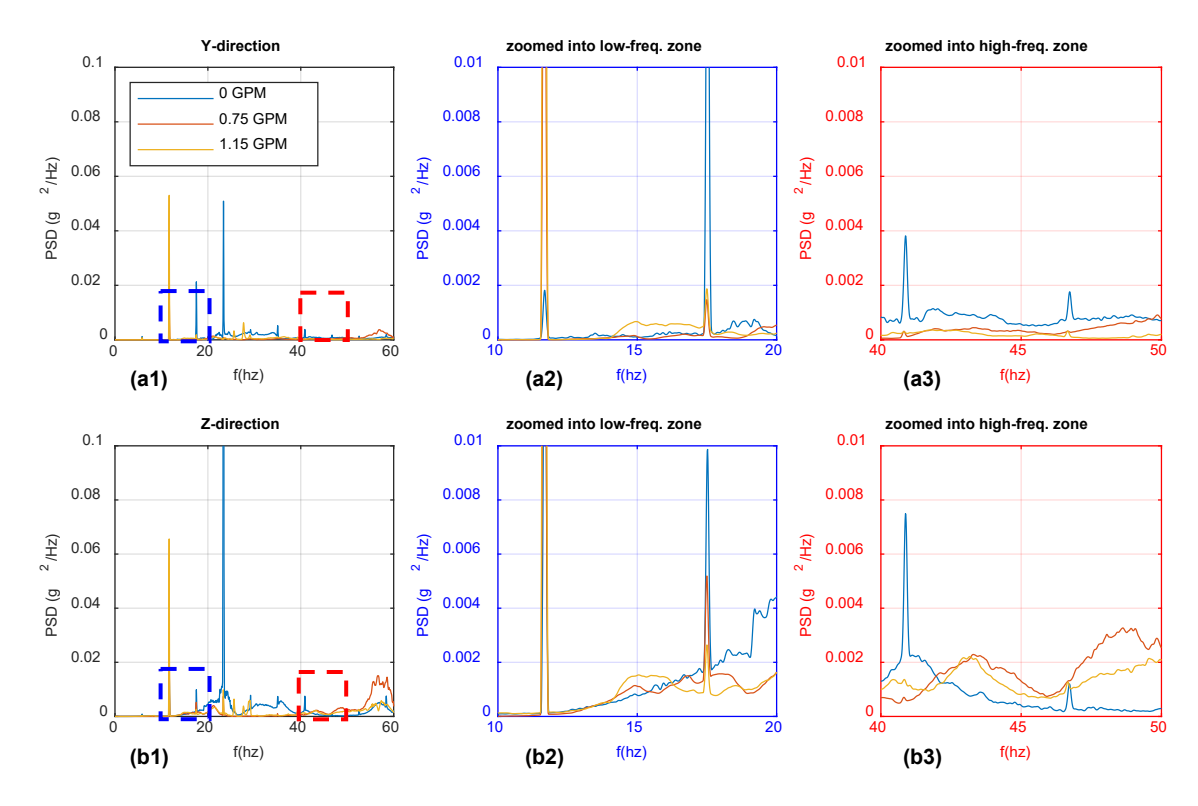


Figure 13 - Case 5 - Lateral acceleration Power Spectral Density (PSD) response for different flow rates in the y & z direction

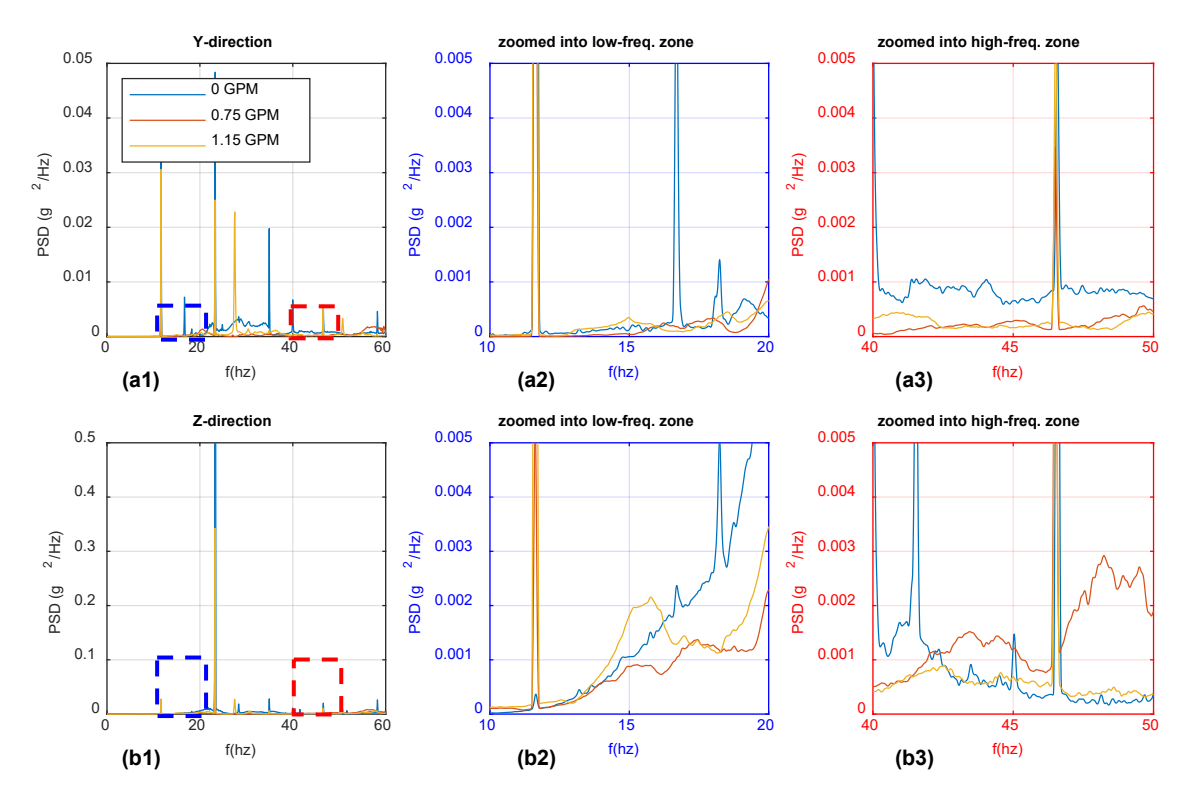


Figure 14 - Case 6 - Lateral acceleration Power Spectral Density (PSD) response for different flow rates in the y & z direction

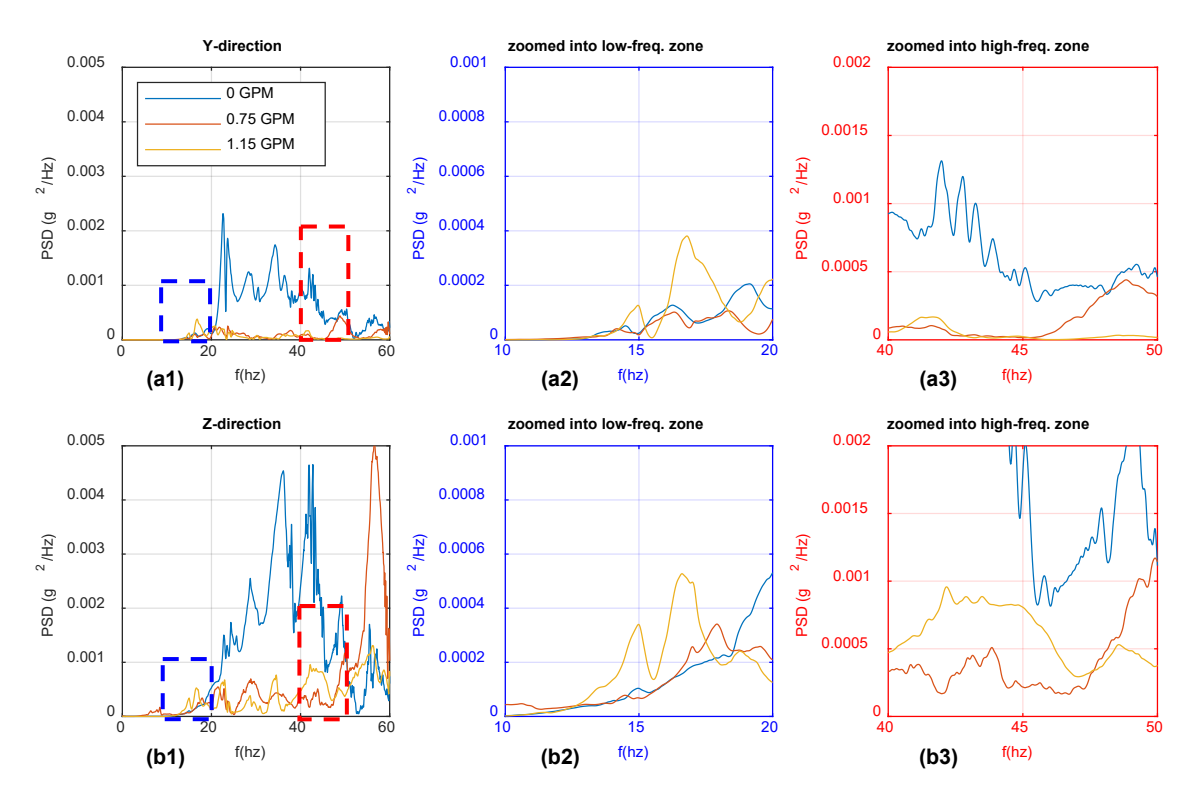


Figure 15 - Case 7 - Lateral acceleration Power Spectral Density (PSD) response for different flow rates in the y & z direction

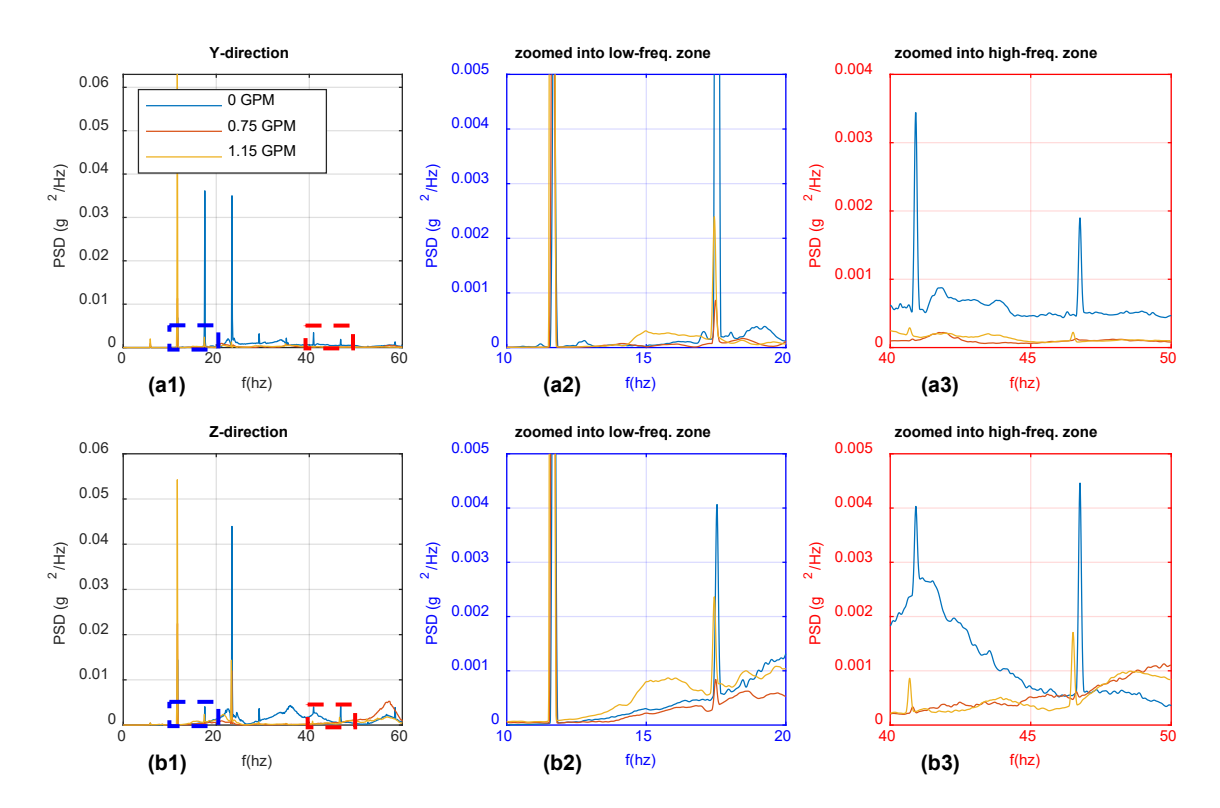


Figure 16 - Case 8 - Lateral acceleration Power Spectral Density (PSD) response for different flow rates in the y & z direction

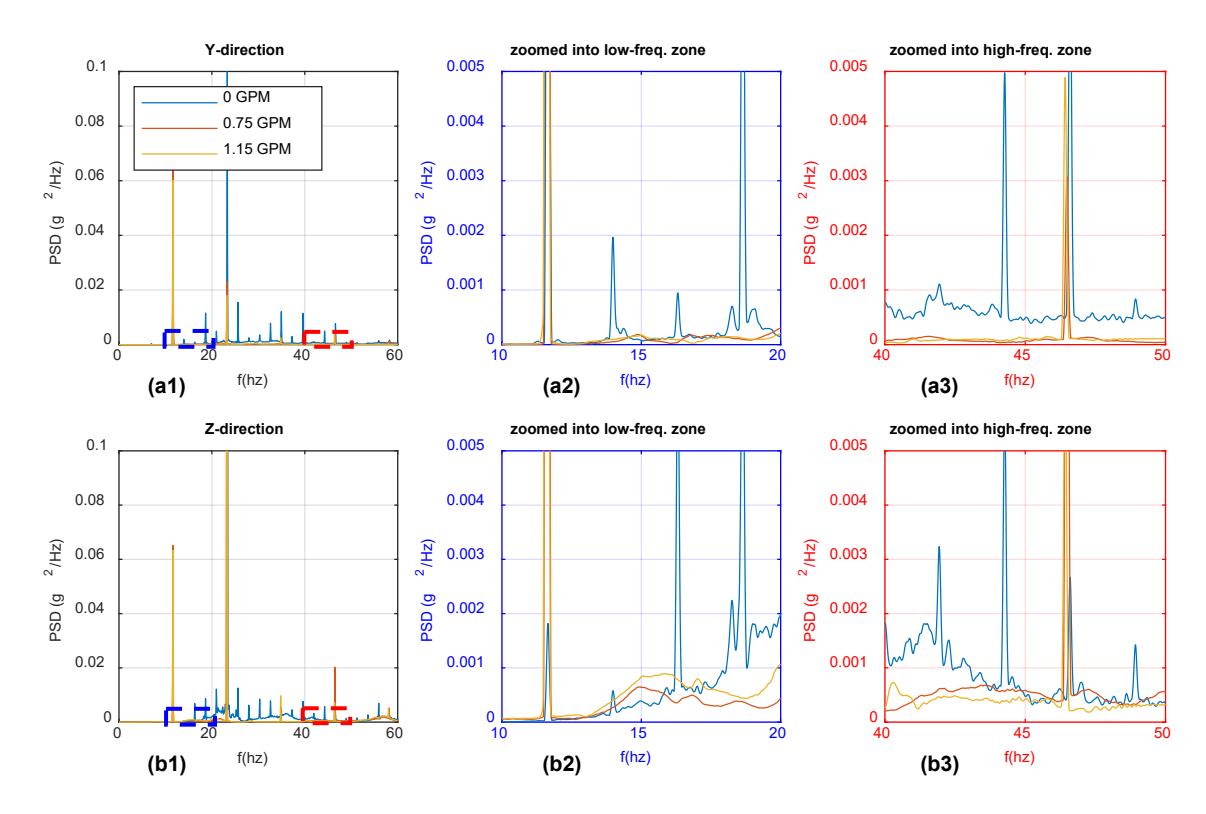


Figure 17 - Case 9 - Lateral acceleration Power Spectral Density (PSD) response for different flow rates in the y & z direction

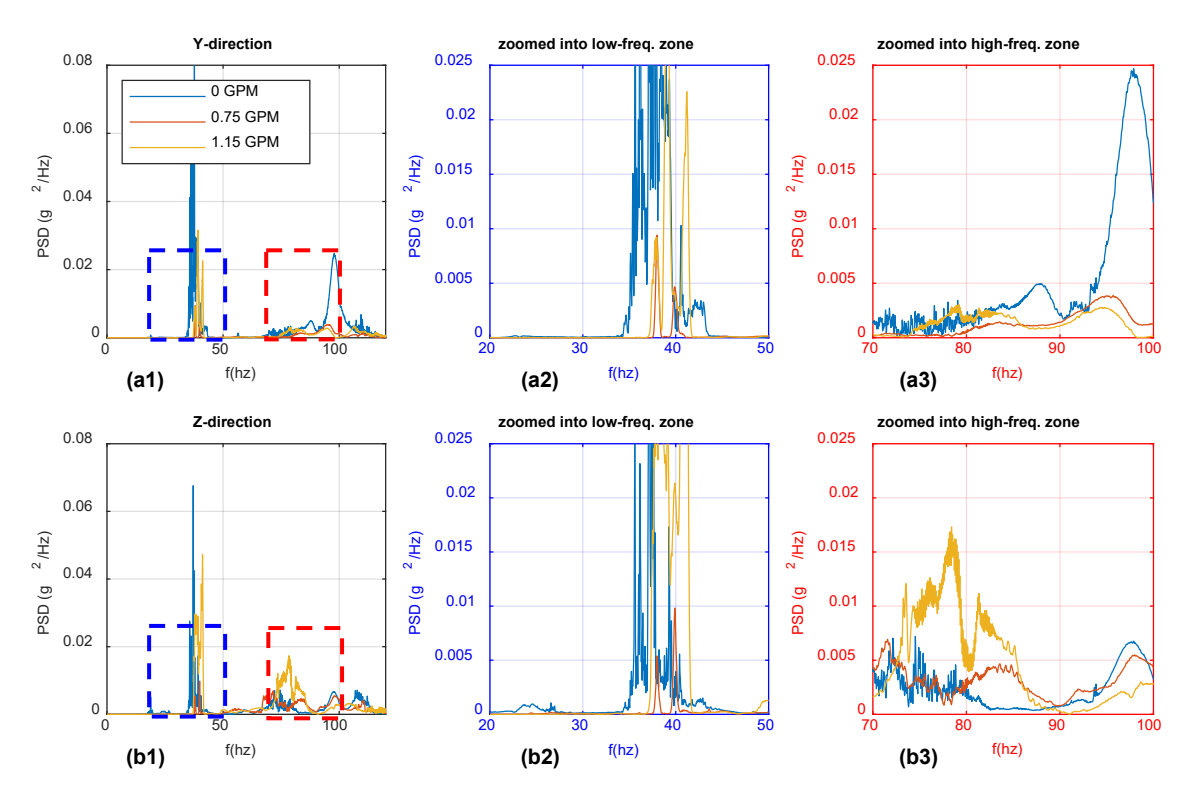


Figure 18 - Case 10 - Lateral acceleration Power Spectral Density (PSD) response for different flow rates in the y & z direction

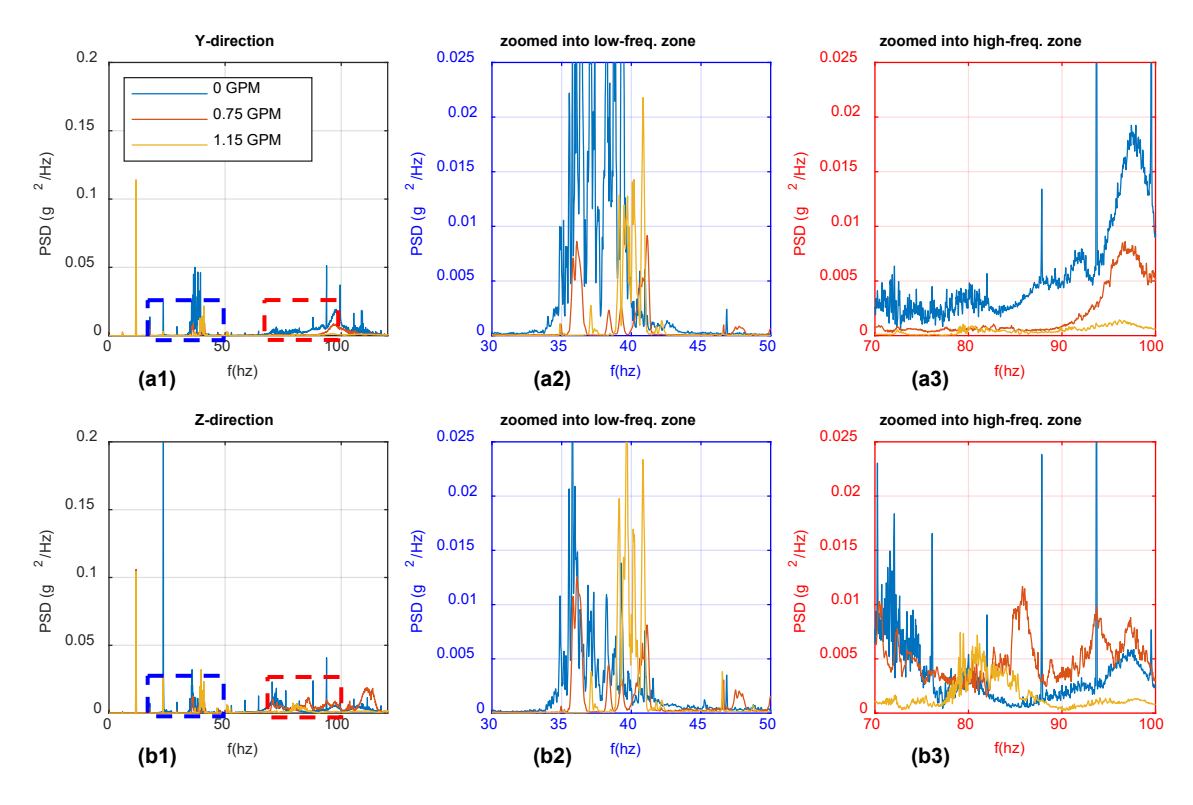


Figure 19 - Case 11 - Lateral acceleration Power Spectral Density (PSD) response for different flow rates in the y & z direction

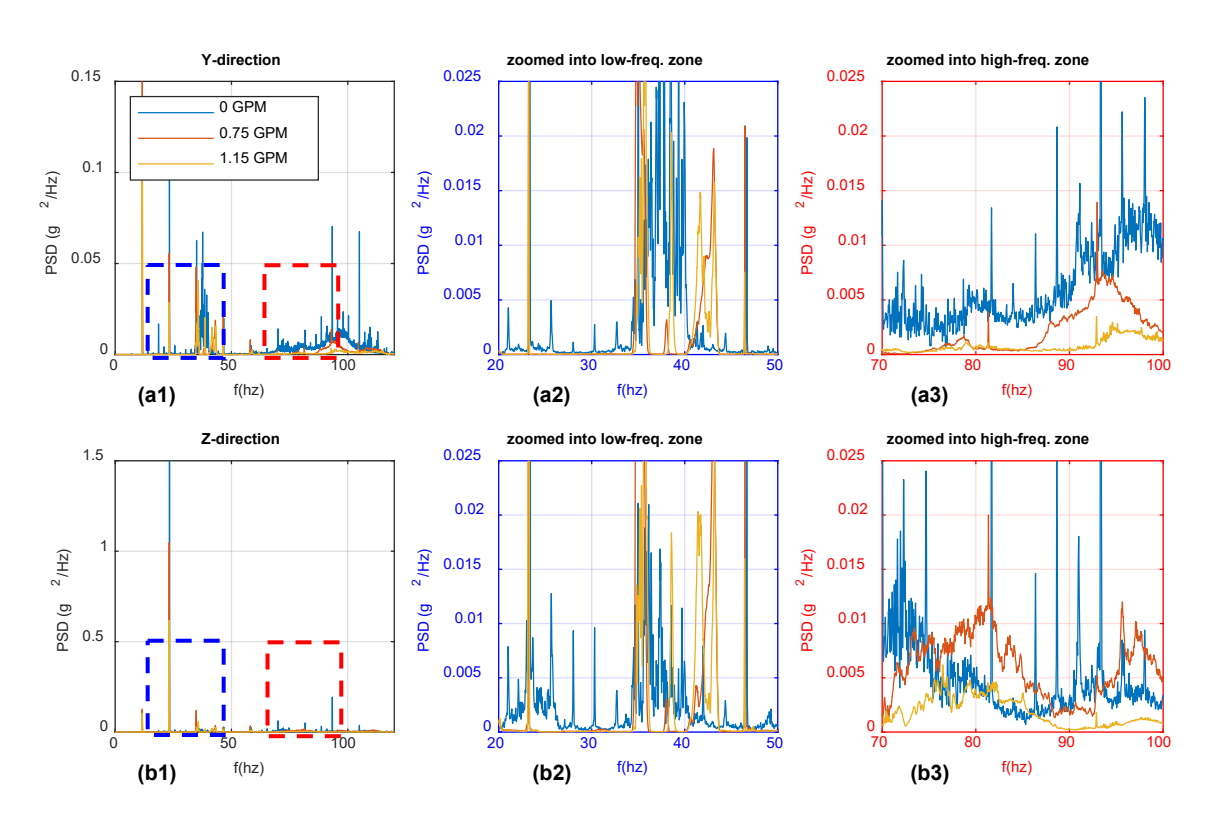


Figure 20 - Case 12 - Lateral acceleration Power Spectral Density (PSD) response for different flow rates in the y & z direction